

Interpolatory Approximations of PMU Data: Dimension Reduction and Pilot Selection

Sean Reiter, Mark Embree, Serkan Gugercin, Vassilis Kekatos, *Senior Member, IEEE*

Abstract—This work investigates the reduction of phasor measurement unit (PMU) data through low-rank matrix approximations. To reconstruct a PMU data matrix from fewer measurements, we propose the framework of interpolatory matrix decompositions (IDs). In contrast to methods relying on principal component analysis or singular value decomposition, IDs recover the complete data matrix using only a few of its rows (PMU datastreams) and/or a few of its columns (snapshots in time). This compression enables the real-time monitoring of power transmission systems using a limited number of measurements, thereby minimizing communication bandwidth. The ID perspective gives a rigorous error bound on the quality of the data compression. We propose selecting rows and columns used in an ID via the discrete empirical interpolation method (DEIM), a greedy algorithm that aims to control the error bound. This bound leads to a computable estimate for the reconstruction error during online operations. A violation of this estimate suggests a change in the system’s operating conditions, and thus serves as a tool for fault detection. Numerical tests using synthetic PMU data illustrate DEIM’s excellent performance for data compression, and validate the proposed DEIM-based fault-detection method.

Index Terms—Low-rank, matrix decomposition, event monitoring, pilot bus, discrete empirical interpolation method (DEIM).

I. INTRODUCTION

Data-driven methods for real-time power system monitoring have garnered significant attention due to the adoption of phasor measurement units (PMUs) in wide-area monitoring systems (WAMS). PMUs are *in situ* sensor devices that provide global positioning system (GPS)-synchronized phasor readings of nodal voltages, nodal currents, line currents, and their time derivatives, at a rate of 60–120 samples per second. These real-time streaming measurements can provide an accurate view of the system’s operating condition, enabling operators to monitor network performance, detect disturbances (such as line trips or outages), and initiate corrective measures. Data accumulation presents a significant roadblock to real-time operational benefits: e.g., a network of 100 PMUs, each with a sampling rate of 120 Hz, generates 200 gigabytes of data per day [1], [2]. Moreover, a large communication bandwidth is required to transmit PMU data to control centers [3]–[5].

This work was supported by US National Science Foundation grants AMPS-1923221 and AMPS-2318800.

Sean Reiter is with the Courant Institute of Mathematical Sciences, New York University, New York, NY USA 10012 (email: s.reiter@nyu.edu).

Mark Embree and Serkan Gugercin are with the Department of Mathematics, Virginia Tech, Blacksburg, VA USA 24061 (email: embree@vt.edu, gugercin@vt.edu).

Vassilis Kekatos is with the Elmore Family School of Electrical and Computer Engineering, Purdue University, West Lafayette, IN USA 47906 (email:kekatos@purdue.edu).

Thus, reliably managing and reducing the scale of streaming PMU data becomes an essential research area.

PMU time series data can be organized in a matrix form: each row corresponds to a single PMU measurement stream, e.g., voltages at a particular bus, and each column contains a snapshot in time. It is well-documented in theory and industry practice that matrices of PMU data exhibit an approximate low-rank structure under both normal and abnormal conditions. This low-rank phenomenon has been attributed to the spatial-temporal correlations in PMU datastreams; see, e.g., [5]–[8]. Data-driven methods exploiting such dependencies in PMU data have been successfully applied to grid monitoring tasks, including detection and localization of disturbance events. Low-rank representations of PMU data are typically computed using methods that decompose the data into orthogonal components, e.g., the singular value decomposition (SVD) [9] or the closely related principal component analysis (PCA) [10]. Event detection algorithms based on PCA are proposed in [11]–[13]. Recognizing the underlying low dimension of PMU data, the authors in [5] propose to monitor a network using fewer pilot PMUs. In [8], low-dimensional subspaces derived from the SVD and subspace comparison metrics are used to identify, detect, and localize events in real time. The papers [14], [15] develop matrix completion-based methods for event detection that use the SVD [14] and arrange PMU data into low-rank Hankel matrices [15]. The paper [16] seeks to express a PMU matrix as a sum of a low-rank matrix, a noise matrix, and a row-sparse matrix that captures abnormal network behavior; this structure is leveraged to detect events. See [7] for a survey of low-rank methods in WAMS.

PCA/SVD provide *optimal* low-rank approximations to the complete PMU matrix by blending information from *all* rows and columns of the PMU matrix, and thus require large amounts of PMU data to be communicated across the network before compression can be applied at a central hub, such as a phasor data concentrator (PDC). Thus, PCA/SVD can be ill-suited for time-sensitive and bandwidth-limited tasks. Moreover, applications such as post-event localization do not explicitly seek an optimal reconstruction of the PMU matrix, but rather aim to reveal a small subset of rows and columns that capture its low-dimensional structure and correspond to points of interest in the grid’s operating history.

As an alternative, we explore *interpolatory matrix decompositions* (IDs) [17]–[21] for the real-time dimension reduction (compression) of PMU data to enable fast and reliable methods for WAMS. In contrast to PCA/SVD, IDs aim to reconstruct the full PMU data matrix using measurements collected from only a small number of PMU datastreams, which

we refer to as *pilot streams* [5], and/or from downsampled time snapshots [3], [4], [22], which we call *pilot snapshots*. While suboptimal in approximation quality, an interpolatory decomposition is more suitable for *real-time* applications. The success of the interpolatory approximation hinges on the choice of pilots, which are identified during an offline training phase. We propose using the *discrete empirical interpolation method* (DEIM) [18], [23]–[26] for adaptively performing this selection. DEIM is a greedy algorithm that aims to minimize a computable upper bound on the interpolatory approximation error. This bound can certify whether a given collection of pilot streams or snapshots truly captures the low-rank character of the data, and can be leveraged for operational uses, such as online error estimation and disturbance event detection.

Our work especially builds on the fundamental contribution of [5], whose authors pursue a similar goal of dimension reduction for real-time event detection. We observe that their method is actually a form of ID, and thus the error bound (14) applies to it. Our approach differs in its general framework based on IDs and in the way it selects pilots. By using DEIM, we seek to control the error bound, so much so that (14) can serve as a viable error indicator for online operations.

Contributions. The key contributions of this work are:

- Introducing IDs as a unified framework for compressing PMU data from a few rows and/or columns, thus leveraging the error measure (12) for certifying IDs for PMUs;
- Proposing the use of the discrete empirical interpolation method (DEIM) for selecting pilot streams and snapshots;
- Adapting the error measure (12) into an indicator for event detection during online operations;
- Applying DEIM to post-event data to locate faults.

Organization. We review the basics of IDs in the context of PMU data reduction in Section II, and describe how these low-rank methods can be used for the real-time reconstruction of streaming PMU data. Section III introduces DEIM for selecting the pilots that determine the ID. Building upon [5], in Section IV we describe an ID-DEIM framework for data-driven monitoring of power systems using a reduced set of pilot streams. Numerical tests using synthetically generated PMU data illustrate and validate the proposed methodology.

Notation. Bold lowercase and uppercase letters $\mathbf{x} \in \mathbb{R}^n$ and $\mathbf{X} \in \mathbb{R}^{n_1 \times n_2}$ denote vectors and matrices. We use MATLAB notation to index: the (i, j) -th entry of \mathbf{X} is denoted $\mathbf{X}(i, j) \in \mathbb{R}$; the i -th row of \mathbf{X} is $\mathbf{X}(i, :) \in \mathbb{R}^{1 \times n_2}$; the j -th column of \mathbf{X} is $\mathbf{X}(:, j) \in \mathbb{R}^{n_1}$ and occasionally $\mathbf{x}_j \in \mathbb{R}^{n_1}$. Given a set of indices $\mathcal{K} = \{k_1, \dots, k_m\}$, let $\mathbf{X}(:, \mathcal{K}) \in \mathbb{R}^{n_1 \times m}$ and $\mathbf{X}(\mathcal{K}, :) \in \mathbb{R}^{m \times n_2}$ denote the columns and rows of \mathbf{X} indexed by \mathcal{K} , and $m = |\mathcal{K}|$ denote the cardinality of \mathcal{K} . With $\mathbf{I}_n \in \mathbb{R}^{n \times n}$, $\mathbf{e}_i \in \mathbb{R}^n$, and $\mathbf{1}_n \in \mathbb{R}^n$ we denote the $n \times n$ identity, the i -th canonical unit vector (\mathbf{e}_i is one in entry i and zero elsewhere), and the vector of all ones. We use $\|\cdot\|_2$ and $\|\cdot\|_F$ to denote the spectral and Frobenius norms of a matrix, and \cdot^\top to denote the vector/matrix transpose.

II. LOW-RANK APPROXIMATION OF PMU MATRICES

Suppose a system operator collects data at T discrete time instances from N PMU datastreams. To simplify the

exposition, assume each measured bus is instrumented with a single PMU. Because each row of a matrix $\mathbf{Y} \in \mathbb{R}^{N \times T}$ containing PMU time series data corresponds to an individual PMU datastream, multiple rows of \mathbf{Y} may be mapped to the same geographic location in the network, e.g., a particular bus. We envision that \mathbf{Y} is typically short and wide ($T > N$) due to the high sampling rate of PMUs, but this is not required; our discussion applies to \mathbf{Y} of arbitrary dimension.

The underlying dimension of PMU data has been considered from a variety of perspectives; see, e.g. [3]–[8], [15]. Matrices of PMU data typically exhibit an underlying low-rank structure, regardless of whether the data are collected during ambient or irregular operating conditions. As a result, the underlying dimension (rank) of \mathbf{Y} can be reduced by retaining only its dominant components computed via PCA [10] or the SVD [9, Sect. 2.4]. The low-rank factors can be stored more efficiently, and any subsequent computations and analysis involving the reconstructed data can be expedited.

A. Approximations of PMU Data via the SVD/PCA

We briefly review how one can obtain a low-rank matrix approximating \mathbf{Y} by truncating the trailing components of its SVD. Define $R = \text{rank}(\mathbf{Y}) \leq \min\{N, T\}$. The SVD of \mathbf{Y} is given by

$$\mathbf{Y} = \mathbf{U}\Sigma\mathbf{V}^\top = \sum_{k=1}^R \sigma_k \mathbf{u}_k \mathbf{v}_k^\top \quad (1)$$

where the diagonal matrix $\Sigma \in \mathbb{R}^{R \times R}$ carries the singular values $\sigma_1 \geq \sigma_2 \geq \dots \geq \sigma_R > 0$, and matrices $\mathbf{U} \in \mathbb{R}^{N \times R}$ and $\mathbf{V} \in \mathbb{R}^{T \times R}$ have orthonormal columns $\mathbf{u}_1, \dots, \mathbf{u}_R$ and $\mathbf{v}_1, \dots, \mathbf{v}_R$ called the left and right singular vectors.

Because real-world PMU data are corrupted by noise, \mathbf{Y} typically has full rank $R = \min(N, T)$. Nonetheless, it can be approximated well by a matrix of lower rank $K \ll R$ obtained from the leading terms in the SVD. By the Eckart–Young–Mirsky theorem [9, Thm. 2.4.8], an optimal rank $K < R$ approximation to \mathbf{Y} in the spectral and Frobenius norms is

$$\mathbf{Y}_K := \mathbf{U}_K \Sigma_K \mathbf{V}_K^\top = \sum_{k=1}^K \sigma_k \mathbf{u}_k \mathbf{v}_k^\top \quad (2)$$

obtained by summing the leading rank-one components $\sigma_k \mathbf{u}_k \mathbf{v}_k^\top$ corresponding to the largest K singular values. Here $\mathbf{U}_K \in \mathbb{R}^{N \times K}$, $\Sigma_K \in \mathbb{R}^{K \times K}$, and $\mathbf{V}_K \in \mathbb{R}^{T \times K}$ are the submatrices of \mathbf{U} , Σ , and \mathbf{V} associated with those leading K singular values. The matrix \mathbf{Y}_K solves

$$\mathbf{Y}_K = \arg \min_{\mathbf{Z} \in \mathbb{R}^{N \times T}} \|\mathbf{Y} - \mathbf{Z}\| \text{ subj. to } \text{rank}(\mathbf{Z}) \leq K$$

where $\|\cdot\|$ can be the spectral or the Frobenius matrix norm. This minimizer attains the approximation errors

$$\|\mathbf{Y} - \mathbf{Y}_K\|_2 = \sigma_{K+1} \text{ and } \|\mathbf{Y} - \mathbf{Y}_K\|_F^2 = \sum_{k=K+1}^R \sigma_k^2. \quad (3)$$

Evidently, \mathbf{Y}_K approximates \mathbf{Y} well if the $R - K$ trailing singular values are sufficiently small. In practice, the rank K

is selected to deliver a relative approximation error below a certain threshold $0 < \alpha < 1$; for example, pick K so that

$$\frac{\|\mathbf{Y} - \mathbf{Y}_K\|_F}{\|\mathbf{Y}\|_F} = \frac{\left(\sum_{k=K+1}^R \sigma_k^2\right)^{1/2}}{\left(\sum_{k=1}^R \sigma_k^2\right)^{1/2}} \leq \alpha. \quad (4)$$

This compression via the SVD is akin to keeping the K principal components of a matrix, as practiced in [5].¹

As noted in the introduction, the SVD blends information from *all* PMU datastreams at *all* times. Because PMUs have limited capacity for handling data, measurements from every datastream must first be transmitted across dedicated synchrophasor communication links before the SVD can be applied to reduce the dimension of the data. Thus, the SVD is not typically feasible for time-sensitive applications involving large-scale systems and is better suited for offline tasks, such as post-event analysis.

B. Interpolatory Approximations of PMU Data

As an alternative to PCA/SVD for PMU data, we propose using *interpolatory matrix decompositions* (IDs) [17]–[21]. These low-rank factorizations, sketched in Figure 1, use only a few rows and/or columns of the matrix. For $K \leq N$, an ID of $\mathbf{Y} \in \mathbb{R}^{N \times T}$ is a low-rank factorization of the form

$$\mathbf{Y} \approx \mathbf{Y}_S^\mathcal{T} := \mathbf{C}^\mathcal{T} \mathbf{X}_S^\mathcal{T} \mathbf{R}_S \quad (5)$$

where $\mathbf{X}_S^\mathcal{T} \in \mathbb{R}^{K \times K}$. The matrices $\mathbf{C}^\mathcal{T} := \mathbf{Y}(:, \mathcal{T}) \in \mathbb{R}^{N \times K}$ and $\mathbf{R}_S := \mathbf{Y}(\mathcal{S}, :) \in \mathbb{R}^{K \times T}$ contain a subset of the columns and rows of \mathbf{Y} indexed by $\mathcal{T} = \{t_1, t_2, \dots, t_K\} \subset \{1, 2, \dots, T\}$ and $\mathcal{S} = \{s_1, s_2, \dots, s_K\} \subset \{1, 2, \dots, N\}$. We refer to the PMU datastreams and time snapshots corresponding to the indices \mathcal{S} and \mathcal{T} as *pilot streams* and *pilot snapshots*, respectively, or simply *pilots* when referring to both. The ID in (5) aims to recover the complete matrix \mathbf{Y} using only information contained in the selected columns $\mathbf{C}^\mathcal{T}$ and rows \mathbf{R}_S of \mathbf{Y} ; the matrix $\mathbf{X}_S^\mathcal{T}$ of smaller dimension $K \times K$ is chosen to make $\mathbf{Y}_S^\mathcal{T}$ a good approximation of \mathbf{Y} .

The approximation quality hinges on which rows and columns are selected for \mathbf{R}_S and $\mathbf{C}^\mathcal{T}$, and the choice for $\mathbf{X}_S^\mathcal{T}$. In Section II-C, we describe a strategy for computing $\mathbf{X}_S^\mathcal{T}$ via a least-squares fit of the data, once \mathcal{S} and \mathcal{T} are set. The numerical linear algebra literature has explored various strategies for selecting rows \mathcal{S} and columns \mathcal{T} ; see, e.g., [17]–[20]. In Section III, we use a greedy strategy from [23], [24] to select rows and columns iteratively.

The form (5) is the most general; one may also consider IDs that only use the rows *or* columns of \mathbf{Y} . Utilizing only certain rows of \mathbf{Y} amounts to using data collected from $K \leq N$ pilot datastreams contained in \mathbf{R}_S to approximate the data from all datastreams, i.e., finding a matrix $\mathbf{Z}_S \in \mathbb{R}^{N \times K}$ such that

$$\mathbf{Y} \approx \mathbf{Y}_S := \mathbf{Z}_S \mathbf{R}_S \in \mathbb{R}^{N \times T}. \quad (6)$$

Note that in (6), columns of \mathbf{Y} are not factored into the approximation. The i -th row of \mathbf{Z}_S contains the weights that

¹Strictly speaking, the data would first be prepared for PCA by subtracting the mean of each row from every entry in that row, replacing \mathbf{Y} with $\mathbf{Y} - \mu_{\mathbf{Y}}^\top$, where $\mu_j = (y_{j,1} + \dots + y_{j,T})/T$. We do not apply any such preprocessing of \mathbf{Y} , and thus take PCA to be synonymous with the SVD.

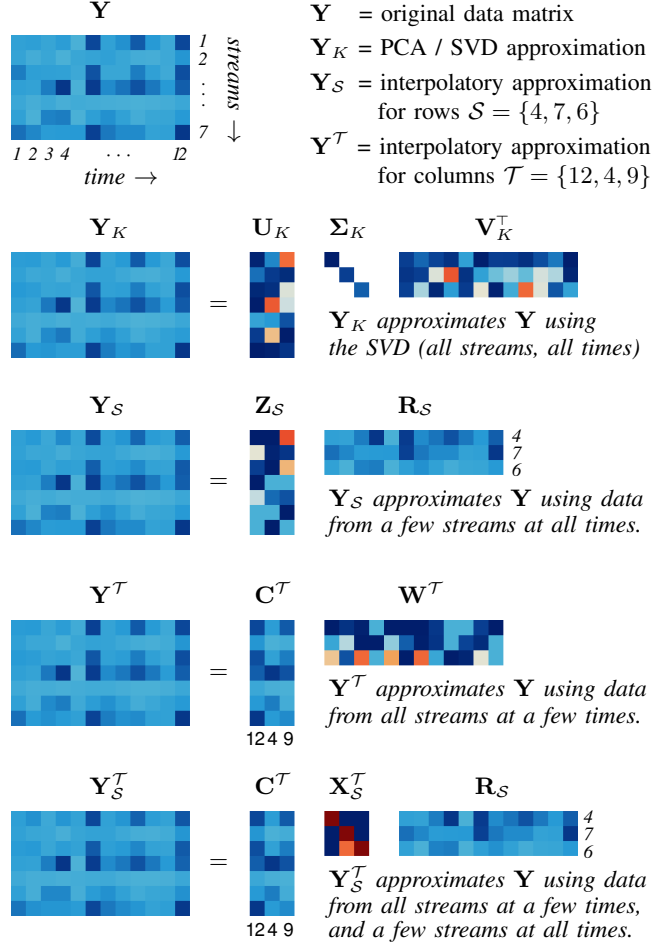


Figure 1: Sketch of four low-rank approximations (\mathbf{Y}_K , \mathbf{Y}_S , $\mathbf{Y}^\mathcal{T}$, and $\mathbf{Y}_S^\mathcal{T}$) to the PMU data matrix \mathbf{Y} . The bottom three are IDs.

specify how the data collected from the K pilot streams in \mathbf{R}_S should be combined to approximate the data $\mathbf{Y}(i, :)$ from the i -th *non-pilot* datastream, $i \notin \mathcal{S}$:

$$\mathbf{Y}(i, :) \approx (\mathbf{Z}_S \mathbf{R}_S)(i, :) = \sum_{k=1}^K \mathbf{Z}_S(i, k) \mathbf{R}_S(k, :). \quad (7)$$

Using only certain columns of \mathbf{Y} amounts to using the $K \leq T$ pilot snapshots contained in $\mathbf{C}^\mathcal{T}$ to recover the full time series, i.e., finding a matrix $\mathbf{W}^\mathcal{T} \in \mathbb{R}^{K \times T}$ such that

$$\mathbf{Y} \approx \mathbf{Y}^\mathcal{T} := \mathbf{C}^\mathcal{T} \mathbf{W}^\mathcal{T} \in \mathbb{R}^{N \times T}. \quad (8)$$

Now the j -th column of $\mathbf{W}^\mathcal{T}$ contains the weights that describe how the selected pilot snapshots in $\mathbf{C}^\mathcal{T}$ should be combined to produce an approximation of the data $\mathbf{Y}(:, j)$ at time t_j for $j \notin \mathcal{T}$, i.e.,

$$\mathbf{Y}(:, j) \approx (\mathbf{C}^\mathcal{T} \mathbf{W}^\mathcal{T})(:, j) = \sum_{k=1}^K \mathbf{W}^\mathcal{T}(j, k) \mathbf{C}^\mathcal{T}(:, k). \quad (9)$$

Figure 1 compares different ID regimes to the SVD. The storage requirements for $\mathbf{C}^\mathcal{T}$, $\mathbf{X}_S^\mathcal{T}$, and \mathbf{R}_S are similar to that of the SVD. Like the optimal approximation \mathbf{Y}_K from the SVD, the interpolatory approximations $\mathbf{Y}_S^\mathcal{T}$, \mathbf{Y}_S , and $\mathbf{Y}^\mathcal{T}$ have rank K (or less). Unlike the orthogonal components \mathbf{U}_K and

\mathbf{V}_K in the SVD, the low-rank factors \mathbf{R}_S and \mathbf{C}^T contain actual PMU data. These factors preserve qualitative features of the data; e.g., sparsity, or a particular voltage pattern if the data was collected following a disturbance [16].

Another virtue of the interpolatory approximations over \mathbf{Y}_K is economy: \mathbf{Y}_K is a blend of *all* $N \gg K$ rows and $T \gg K$ columns of \mathbf{Y} , so computing the SVD requires information from *all* PMU time series simultaneously. On the other hand, interpolatory approximations \mathbf{Y}_S and \mathbf{Y}^T only use $K = |\mathcal{S}| = |\mathcal{T}|$ rows and columns of \mathbf{Y} . Once the weights \mathbf{Z}_S and \mathbf{W}^T have been computed, a low-rank approximation to \mathbf{Y} can be obtained while interacting *only* with $K \leq N$ pilot streams or $K \leq T$ down-sampled pilot snapshots. As observed in, e.g., [3]–[5], this reduction significantly lowers the bandwidth needs of synchrophasor communication networks. We point out that the sparse approximations of PMU data proposed in [3]–[5], [22] can be interpreted at the matrix level as one-sided interpolatory approximations (6) and (8).

C. Analyzing the Interpolatory Approximation Error

Because \mathbf{Y}_K is the optimal rank- K approximation to \mathbf{Y} , the interpolatory approximation \mathbf{Y}_S^T cannot be any better:

$$\sigma_{K+1} = \|\mathbf{Y} - \mathbf{Y}_K\|_2 \leq \|\mathbf{Y} - \mathbf{Y}_S^T\|_2. \quad (10)$$

The same holds for \mathbf{Y}_S and \mathbf{Y}^T . How close is \mathbf{Y}_S^T to the best approximation from PCA/SVD? For the moment, we assume the K row and column indices in \mathcal{S} and \mathcal{T} are given. The error $\|\mathbf{Y} - \mathbf{Y}_S^T\|_2$ depends on how we compute \mathbf{X}_S^T . One natural choice [17], [21] is

$$\mathbf{X}_S^T = (\mathbf{C}^T)^\dagger \mathbf{Y} (\mathbf{R}_S)^\dagger$$

where \cdot^\dagger denotes the *Moore–Penrose pseudoinverse* [9, Section 5.5.2]. Assuming the rows of \mathbf{R}_S and the columns of \mathbf{C}^T are linearly independent, we have $(\mathbf{R}_S)^\dagger = \mathbf{R}_S^\top (\mathbf{R}_S \mathbf{R}_S^\top)^{-1}$ and $(\mathbf{C}^T)^\dagger = (\mathbf{C}^{T\top} \mathbf{C}^T)^{-1} \mathbf{C}^{T\top}$. Thus, \mathbf{Y}_S^T is given by

$$\mathbf{Y}_S^T = \mathbf{C}^T \mathbf{X}_S^T \mathbf{R}_S = \mathbf{C}^T (\mathbf{C}^T)^\dagger \mathbf{Y} (\mathbf{R}_S)^\dagger \mathbf{R}_S.$$

For the one-sided interpolatory approximations \mathbf{Y}_S and \mathbf{Y}^T , the same idea can be applied to obtain \mathbf{Z}_S and \mathbf{W}^T :

$$\mathbf{W}^T = (\mathbf{C}^T)^\dagger \mathbf{Y} \quad \text{and} \quad \mathbf{Z}_S = \mathbf{Y} (\mathbf{R}_S)^\dagger.$$

This construction highlights why IDs can effectively compress the entire PMU data set in \mathbf{Y} : the matrices \mathbf{Z}_S and \mathbf{W}^T are least squares fits of the data [21], e.g.,

$$\mathbf{Z}_S = \arg \min_{\mathbf{Z} \in \mathbb{R}^{N \times K}} \|\mathbf{Y} - \mathbf{Z} \mathbf{R}_S\|_F. \quad (11)$$

Assuming the rows (columns) of \mathbf{Y} are linearly independent, the solutions \mathbf{Z}_S (\mathbf{W}^T) to (11) are unique. The pilot-based reconstruction from [5] in fact uses this choice of \mathbf{Z}_S .

The quality of the IDs \mathbf{Y}_S^T , \mathbf{Y}_S , and \mathbf{Y}^T can be assessed in a more quantitative way. Define $\mathbf{S} := \mathbf{I}_N(:, \mathcal{S}) \in \mathbb{R}^{N \times K}$ and $\mathbf{T} := \mathbf{I}_T(:, \mathcal{T}) \in \mathbb{R}^{T \times K}$ to be the matrices containing the K columns of the $N \times N$ and $T \times T$ identity matrices indexed by \mathcal{S} and \mathcal{T} . From [18, Theorem 4.1], we have that

$$\sigma_{K+1} \leq \|\mathbf{Y} - \mathbf{Y}_S^T\|_2 \leq (\eta_S + \eta_T) \sigma_{K+1} \quad (12)$$

where error factors $\eta_S, \eta_T \geq 1$ are given by

$$\eta_S := \|(\mathbf{S}^\top \mathbf{U}_K)^{-1}\|_2 \quad \text{and} \quad \eta_T := \|(\mathbf{T}^\top \mathbf{V}_K)^{-1}\|_2. \quad (13)$$

Recall that $\mathbf{U}_K \in \mathbb{R}^{N \times K}$ and $\mathbf{V}_K \in \mathbb{R}^{T \times K}$ contain the leading K left and right singular vectors of \mathbf{Y} . The submatrices $\mathbf{S}^\top \mathbf{U}_K$ and $\mathbf{T}^\top \mathbf{V}_K$ are guaranteed to be nonsingular for certain row and column selection schemes, including the one we propose in Section III; see [18, Lemma 3.2]. For the one-sided interpolatory approximations \mathbf{Y}_S and \mathbf{Y}^T , we have the simplified bounds:

$$\begin{aligned} \sigma_{K+1} &\leq \|\mathbf{Y} - \mathbf{Y}_S\|_2 \leq \eta_S \sigma_{K+1} \\ \sigma_{K+1} &\leq \|\mathbf{Y} - \mathbf{Y}^T\|_2 \leq \eta_T \sigma_{K+1}. \end{aligned} \quad (14)$$

See [18, Lemma 4.2] and [27, Theorem 1.5].

Let us unpack the error factors η_S and η_T . The matrix $\mathbf{S}^\top \mathbf{U}_K$ is a $K \times K$ submatrix of \mathbf{U}_K . Note that \mathbf{U}_k has orthonormal columns; η_S measures how far from orthonormal the *rows* of \mathbf{U}_K corresponding to \mathcal{S} are. Likewise, η_T measures how far from orthonormal the \mathcal{T} rows of \mathbf{V}_K are. The order of the indices in \mathcal{S} and \mathcal{T} does not affect η_S and η_T .

The interpolatory error bounds in (12) and (14) hold for *any* collection of pilot indices \mathcal{S} or \mathcal{T} . We can leverage these bounds to realize real-time computational benefits and performance guarantees. Although these ideas also apply to the two-sided formulation in (5), we present them for the one-sided approximations (6) and (8) for simplicity.

1. *Fast error monitoring.* Because $\mathbf{S}^\top \mathbf{U}_K$ and $\mathbf{T}^\top \mathbf{V}_K$ are small $K \times K$ matrices, the error indicators η_S and η_T will be much quicker to compute than the full approximation errors $\|\mathbf{Y} - \mathbf{Y}_S\|_2$ or $\|\mathbf{Y} - \mathbf{Y}^T\|_2$ for large N and T . One does not even need to explicitly form the low-rank approximations \mathbf{Y}_S or \mathbf{Y}^T in (6) and (8), and hence \mathbf{Z}_S or \mathbf{W}^T , to evaluate η_S and η_T . This observation allows for fast *a priori* estimation of the interpolatory approximation error during online operations, or enables the error factors to be monitored as the pilots are selected.

2. *Pilot certification.* In an operational setting, one can use any desired strategy for picking pilots \mathcal{S} and \mathcal{T} . The error factors η_S or η_T can then be (quickly) computed to certify if the chosen pilots capture the rank- K nature of the PMU data matrix. If the error bound is below a threshold, e.g., $\eta_S \sigma_{K+1}, \eta_T \sigma_{K+1} \leq \tau = 10^{-1}$, the selection \mathcal{S} or \mathcal{T} is accepted; otherwise, either replace some pilots, or increase K and add additional pilots.

We describe at length how each of the above ideas can be implemented in a practical operational scenario in Section IV.

One could consider selecting pilots \mathcal{S} and \mathcal{T} to explicitly minimize η_S and η_T over all possible configurations; however, such a minimization would involve combinatorial complexity. Instead, in Section III we advocate for a more efficient *greedy* algorithm that seeks to control the growth of the error factors η_S and η_T as new pilots are selected, one at a time.

III. GREEDY PILOT SELECTION

We propose using the *discrete empirical interpolation method* (DEIM) index selection algorithm [18], [23]–[26] to select the pilot subsets \mathcal{S} and \mathcal{T} . DEIM is a discrete

variant of the empirical interpolation method [24]. Initially developed for resolving the “lifting bottleneck” in the model reduction of nonlinear dynamical systems [23] by constructing interpolatory approximations to vector-valued nonlinear functions, DEIM was applied to construct IDs in [18]. The DEIM procedure (independently) selects the row and column indices \mathcal{S} and \mathcal{T} by iteratively parsing the leading left and right singular vectors stored in \mathbf{U}_K and \mathbf{V}_K for a matrix \mathbf{Y} . At each iteration, DEIM attempts to adaptively minimize the growth of the error factors in (13) as each new index is added to \mathcal{S} or \mathcal{T} , and, in practice, the DEIM indices typically yield small error factors. In the numerical tests of Section IV, DEIM selects pilot configurations that produce error factors $\eta_{\mathcal{S}}$ and $\eta_{\mathcal{T}}$ of size $\mathcal{O}(10^1)$ or less, whereas other, seemingly reliable, selection approaches produce factors of size $\mathcal{O}(10^4)$. Thus, in conjunction with the approximation error (12), we expect DEIM to provide an effective pilot selection strategy.

A. The Discrete Empirical Interpolation Method

We describe how DEIM operates on \mathbf{U}_K to select $K \leq N$ pilot streams \mathcal{S} from a data matrix \mathbf{Y} . The same process applied (independently) to \mathbf{V}_K selects the pilot snapshots \mathcal{T} .

Our derivation uses special matrices called *interpolatory projectors*. Let $\mathbf{S}_k = [\mathbf{e}_{s_1} \dots \mathbf{e}_{s_k}] \in \mathbb{R}^{N \times k}$ denote the k columns of \mathbf{I}_N specified by the distinct indices in $\mathcal{S}_k = \{s_1, \dots, s_k\} \subset \{1, \dots, N\}$, and let $\mathbf{U}_k = \mathbf{U}(:, 1:k) = [\mathbf{u}_1 \dots \mathbf{u}_k] \in \mathbb{R}^{N \times k}$ denote the leading k columns of the matrix $\mathbf{U} \in \mathbb{R}^{N \times R}$ of the left singular vectors of \mathbf{Y} . The *interpolatory projector* for \mathcal{S}_k onto $\text{span}(\mathbf{U}_k)$ is defined as

$$\mathbf{P}_k := \mathbf{U}_k (\mathbf{S}_k^T \mathbf{U}_k)^{-1} \mathbf{S}_k^T \in \mathbb{R}^{N \times N}. \quad (15)$$

The matrix $\mathbf{S}_k^T \mathbf{U}_k \in \mathbb{R}^{k \times k}$ is guaranteed to be invertible for indices \mathcal{S}_k adaptively selected by DEIM [18, Lemma 3.2]. One can readily verify that \mathbf{P}_k satisfies the projector property: $\mathbf{P}_k^2 = \mathbf{P}_k$. More critically, \mathbf{P}_k is an *interpolatory projector* in this sense: for any vector $\mathbf{x} \in \mathbb{R}^N$, the projected vector $\hat{\mathbf{x}} := \mathbf{P}_k \mathbf{x}$ exactly matches \mathbf{x} in the pilot indices \mathcal{S}_k , i.e.,

$$\hat{\mathbf{x}}(\mathcal{S}_k) = \mathbf{S}_k^T (\mathbf{U}_k (\mathbf{S}_k^T \mathbf{U}_k)^{-1} \mathbf{S}_k^T) \mathbf{x} = \mathbf{x}(\mathcal{S}_k). \quad (16)$$

DEIM operates on the columns of \mathbf{u}_k one at a time to select each new pilot index. Start with the selection of the first pilot s_1 , corresponding to $k = 1$. In this simple case, the error factor $\eta_{\mathcal{S}_1}$ in (13) reduces to

$$\eta_{\mathcal{S}_1} = \|(\mathbf{S}_1^T \mathbf{U}_1)^{-1}\|_2 = \frac{1}{|\mathbf{u}_1(s_1)|}$$

the reciprocal of the magnitude of the s_1 entry of the leading singular vector \mathbf{u}_1 . Therefore, to minimize $\eta_{\mathcal{S}_1}$, choose the datastream index $s_1 \in \{1, \dots, N\}$ corresponding to the entry in $\mathbf{u}_1 \in \mathbb{R}^N$ having the largest magnitude.

- **Step 1.** Choose s_1 as the index corresponding to the entry of \mathbf{u}_1 with the largest magnitude:

$$s_1 = \arg \max_{1 \leq s \leq N} |\mathbf{u}_1(s)|, \quad \mathbf{u}_1 = \begin{bmatrix} \times \\ \textcolor{red}{\times} \\ \times \\ \times \end{bmatrix} \leftarrow s_1.$$

Construct $\mathbf{P}_1 := \mathbf{u}_1 \mathbf{e}_{s_1}^T / |\mathbf{u}_1(s_1)|$, the interpolatory projector (15) for $\mathcal{S}_1 = \{s_1\}$ onto the span of \mathbf{u}_1 .

The choice of the second index s_2 is more subtle. We should avoid choosing the same pilot ($s_2 = s_1$), which would result in an infinite error factor $\eta_{\mathcal{S}} = \|(\mathbf{S}_2^T \mathbf{U}_2)^{-1}\|_2$. Using the intuition that $\eta_{\mathcal{S}} = \|(\mathbf{S}_k^T \mathbf{U}_k)^{-1}\|_2$ is small when the rows of \mathbf{U}_k selected by \mathbf{S}_k are quite distinct, we choose s_2 so that the two rows $\mathbf{U}_2(\mathcal{S}_2, :)$ are as *independent as possible* for $\mathcal{S}_2 = \{s_1, s_2\}$. To guarantee that $s_2 \neq s_1$, i.e., that we select a distinct datastream, we remove a multiple of \mathbf{u}_1 from \mathbf{u}_2 to zero out the s_1 entry:

$$\mathbf{r}_2 := \mathbf{u}_2 - \frac{\mathbf{u}_2(s_1)}{\mathbf{u}_1(s_1)} \mathbf{u}_1 = \mathbf{u}_2 - \mathbf{P}_1 \mathbf{u}_2$$

giving $\mathbf{r}_2(s_1) = 0$ by the interpolatory property of \mathbf{P}_1 in index s_1 . We can then select s_2 to be the index of the largest-magnitude entry of \mathbf{r}_2 . Using this formulation, we summarize the next step of DEIM as follows.

- **Step 2.** Compute the residual of the interpolatory projection of \mathbf{u}_2 onto $\text{span}(\mathbf{u}_1)$:

$$\mathbf{r}_2 = \mathbf{u}_2 - \mathbf{P}_1 \mathbf{u}_2.$$

Choose s_2 as the largest-magnitude entry of \mathbf{r}_2 :

$$s_2 = \arg \max_{1 \leq n \leq N} |\mathbf{r}_2(n)|, \quad \mathbf{r}_2 = \mathbf{u}_2 - \mathbf{P}_1 \mathbf{u}_2 = \begin{bmatrix} \star \\ 0 \\ \star \\ \textcolor{red}{\star} \end{bmatrix} \leftarrow s_2$$

(The \star indicates a modified entry from the $k = 1$ step.)

Subsequent steps, $k = 3, \dots, K$, follow this same template.

- **Step k .** Construct the interpolatory projector \mathbf{P}_{k-1} for datastreams s_1, \dots, s_{k-1} onto the span of $\mathbf{u}_1, \dots, \mathbf{u}_{k-1}$ according to (15), and compute the residual

$$\mathbf{r}_k = \mathbf{u}_k - \mathbf{P}_{k-1} \mathbf{u}_k$$

such that $\mathbf{r}_k(s_1) = \dots = \mathbf{r}_k(s_{k-1}) = 0$. Choose s_k to be the index of the largest-magnitude entry of \mathbf{r}_k :

$$s_k = \arg \max_{1 \leq s \leq N} |\mathbf{r}_k(s)|.$$

We are assured that s_k is a new datastream that differs from s_1, \dots, s_{k-1} , since $\mathbf{r}_k(s_1) = \dots = \mathbf{r}_k(s_{k-1}) = 0$ but $\mathbf{r}_k \neq \mathbf{0}$ (otherwise, $\mathbf{u}_k \in \text{span}\{\mathbf{u}_1, \dots, \mathbf{u}_{k-1}\}$, a contradiction).

Algorithm III.1 summarizes this procedure. (To select pilot snapshots \mathcal{T} , i.e., columns of \mathbf{Y} , simply apply this algorithm to the right singular vectors \mathbf{V}_K .) An efficient implementation avoids explicitly forming the interpolatory projectors \mathbf{P}_k , which are large, dense matrices; rather, step 4 of Algorithm III.1 computes the *action* of \mathbf{P}_k on the singular vector \mathbf{u}_k . At every iteration, the DEIM selection is designed to roughly minimize the incremental growth of the error factor $\eta_{\mathcal{S}}$ in the bound (14); see [23, Lemma 3.2] for a proof. This explains why DEIM is an effective choice for computing the pilot sets \mathcal{S} and \mathcal{T} , as illustrated in [18, Section 6].

The DEIM algorithm is directly linked to the LU factorization with partial pivoting; see [18, Section 3]. One alternative to the DEIM index selection algorithm is the

Algorithm III.1: The discrete empirical interpolation method (DEIM) [23], [24].

Input: Matrix with orthonormal columns
 $\mathbf{U}_K = [\mathbf{u}_1 \ \cdots \ \mathbf{u}_K] \in \mathbb{R}^{N \times K}$, $1 \leq K < N$.
Output: Indices $\mathcal{S} = \{s_1, \dots, s_K\} \subset \{1, \dots, N\}$.
1 Choose the first index $s_1 = \arg \max_{1 \leq s \leq N} |\mathbf{u}_1(s)|$.
2 Take $\mathcal{S}_1 = \{s_1\}$.
3 **for** $k = 2, \dots, K$ **do**
4 Compute the residual by solving a k -dimensional linear system:

$$\mathbf{r}_k = \mathbf{u}_k - \mathbf{U}_{k-1} (\mathbf{S}_{k-1}^\top \mathbf{U}_{k-1})^{-1} \mathbf{S}_{k-1}^\top \mathbf{u}_k.$$

5 Choose $s_k = \arg \max_{1 \leq s \leq N} |\mathbf{r}_k(s)|$.
6 Take $\mathcal{S}_k = \mathcal{S}_{k-1} \cup \{s_k\}$.
7 **end**

QDEIM variant [25], which identifies the pilots \mathcal{S} by applying a rank-revealing QR factorization to the rows of \mathbf{U}_K . The ultimate set of pilots \mathcal{S} chosen by QDEIM is invariant under permutations of the columns of \mathbf{U}_K , although in practice, DEIM and QDEIM perform similarly. (QDEIM is not iterative; the number of desired pilots must be specified in advance.)

B. Numerical Tests

The code and data for reproducing all results are available at [28]. We now demonstrate the ability of the row- and column-based IDs (6) and (8) to reduce the dimension of PMU data matrices using different strategies for selecting the pilots \mathcal{S} and \mathcal{T} . We compare the following selection strategies.

DEIM is Algorithm III.1 from [23], [24].

QDEIM is the QDEIM variant of DEIM from [25].

MILP chooses the indices via a mixed integer linear program (MILP) that aims to choose the rows and columns of \mathbf{Y} to be as orthogonal as possible to each other. This approach is based on the pilot PMU selection strategy proposed in [5, Sec. II]. The program is solved using MATLAB's `intlinprog` command.

RAND is a random selection (MATLAB's `randi` command). These strategies are applied to a matrix \mathbf{Y} of PMU data to identify the sets \mathcal{S} and \mathcal{T} with K indices. Then, matrices \mathbf{Z}_S and $\mathbf{W}^\mathcal{T}$ are computed from (11), and used to form rank- K IDs \mathbf{Y}_S and $\mathbf{Y}^\mathcal{T}$ of the matrix \mathbf{Y} according to (6) and (8). To assess the quality of the reduction, we compute the relative errors induced by \mathbf{Y}_S and $\mathbf{Y}^\mathcal{T}$ in the matrix 2-norm, and compare this against the relative best rank- k approximation error σ_{k+1}/σ_1 from the SVD. We also compute the associated error factors η_S and $\eta_\mathcal{T}$ for each selection strategy.

We test the efficacy of the IDs on synthetic PMU data generated from transient simulations of the NETSNYPS 68-bus, 16-machine test system [29, Ch. 4] using MATLAB's Power Systems Toolbox (PST) [30]. The PMU datastreams are voltage magnitudes collected at every bus at a sampling rate of 100 Hz over a 60 s window; these data are organized as a 68×6000 dimensional matrix \mathbf{Y} . After 30 s of the simulation, a three-phase line fault is applied between buses 28 and 29

and cleared 0.2 s later. To mimic realistic operating conditions and generate noisy voltages, the mechanical power and exciter references of the generators were perturbed by zero-mean Gaussian white noise. For the column-based IDs (8), we do not employ the MILP-based selection because the matrices required for solving the program do not fit in memory.

Figure 2 shows the relative errors in the 2-norm. We compute rank $k = 1, 2, \dots, 20$ row- and column-based IDs for the PMU data \mathbf{Y} using the selection strategies outlined above. The DEIM- and QDEIM-based IDs give results on par with those of the SVD for each rank K . The MILP-based IDs perform poorly after an initial reduction for small K ; the approximation errors oscillate as K increases. The row-based IDs perform better than the column-based ones, as expected, since the column-based approximations have more indices to choose from (6000 vs. 68). These results demonstrate that, when combined with a reliable pilot selection strategy, IDs are an effective tool for reducing the dimension of PMU data.

IV. DATA-DRIVEN MONITORING WITH ID-DEIM

Several works have proposed using changes in the low-dimensional subspace spanned by streaming PMU data to monitor for, detect, and localize system events in real time; see, e.g., [5], [8], [11]–[13], [16], [31]. Here, we propose such a data-driven framework for real-time monitoring based on the IDs presented in Section II and the DEIM index selection algorithm described in Section III. The proposed framework builds upon the online monitoring algorithm presented in [5, Sec. II], insofar as only a reduced number of pilot PMU datastreams are utilized to monitor the network. All non-pilot datastreams in the network are recovered from these pilots, effectively reducing the dimension of the streaming data. In contrast to the work of [5], our algorithm views this dimension reduction through the lens of IDs (6), enabling the use of the interpolatory error bound $\eta_S \sigma_{K+1}$ in (14). This perspective yields a few key operational benefits: Offline, DEIM is applied to select pilot streams \mathcal{S} , increasing the number of pilots K until the bound $\eta_S \sigma_{K+1}$ is less than a user-specified tolerance. Online, $\eta_S \sigma_{K+1}$ serves as an *estimator* of the interpolatory reconstruction error; deterioration of this estimate suggests a change in the operating condition of the network, and can be used as a simple “tripwire” for detecting disturbances. Following such a detection, the DEIM algorithm is applied to the transient system response due to the disturbance to localize the source of the event purely from data, with high accuracy. Numerical tests are interspersed throughout this section to illustrate the proposed framework.

A. Adaptive DEIM-based Training of Pilots

At this point, we differentiate between *offline* training data $\mathbf{Y}_{\text{trn}} \in \mathbb{R}^{N \times T_{\text{trn}}}$ and *online* streaming data $\mathbf{Y}_{\text{obs}} \in \mathbb{R}^{N \times T_{\text{obs}}}$. The positive integers $T_{\text{trn}}, T_{\text{obs}}$ dictate the size of the training and online monitoring windows. The parameter T_{trn} is tunable; in our tests, we choose T_{trn} to correspond to ~ 120 s worth of data collected during normal operating conditions. On the other hand, we take T_{obs} to be fixed, but not necessarily known *a priori*. For the online monitoring portion of the

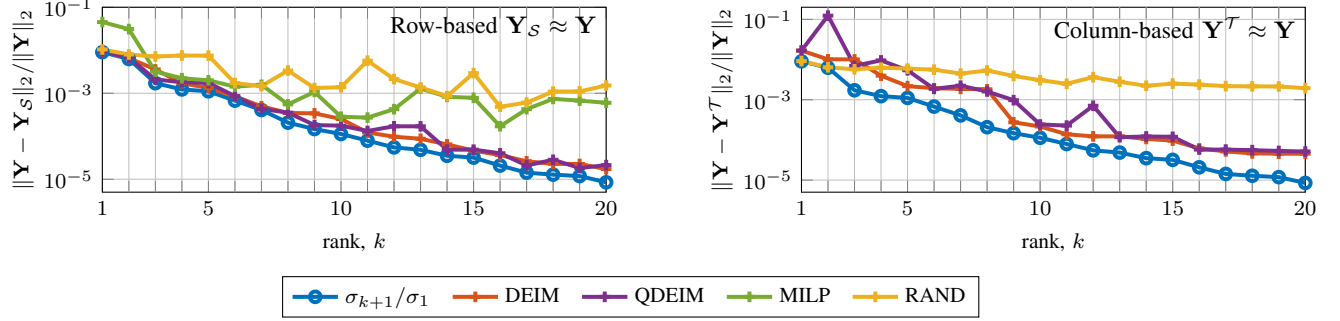


Figure 2: Relative errors for rank $k = 2, 3, \dots, 20$ interpolatory matrix approximations \mathbf{Y}_S and \mathbf{Y}^T of the data matrix $\mathbf{Y} \in \mathbb{R}^{68 \times 6000}$ generated using the 68-bus, 16-machine NETSNYPS test system. The size of the column-based data prevents use of MILP in the right plot.

algorithm, where the full \mathbf{Y}_{obs} is approximated from a few pilot datastreams via an ID $\mathbf{Y}_S = \mathbf{Z}_S \mathbf{R}_S$, two things need to be computed offline from \mathbf{Y}_{trn} to formulate \mathbf{Y}_S :

1. The indices \mathcal{S} corresponding to the pilot datastreams that will form the basis of the ID;
2. The matrix of weights $\mathbf{Z}_S \in \mathbb{R}^{N \times K}$ that encodes how the pilot datastreams in \mathcal{S} should be combined to recover measurements at the non-pilot datastreams.

To choose the pilots in \mathcal{S} , DEIM is applied to the leading left singular vectors of \mathbf{Y}_{trn} until $\eta_S \sigma_{K+1} \leq \tau$, where $\tau > 0$ is a user-specified error tolerance. In our tests, for modest values of τ , e.g., $\tau = 10^{-1}$, the error bound satisfies $\eta_S \sigma_{K+1} \leq \tau$ for small values of K , e.g., $K \leq 5$. A reliable heuristic for tuning τ is provided by the singular values of \mathbf{Y}_{trn} , since σ_{K+1} is the best rank- K approximation error. A smaller tolerance τ necessitates more pilots, giving a tradeoff between reconstruction accuracy and the bandwidth required to communicate across the K pilot. After the pilot streams \mathcal{S} are identified, the matrix \mathbf{Z}_S is computed by solving the least-squares problem (11) with $\mathbf{Y} = \mathbf{Y}_{\text{trn}}$ and $\mathbf{R}_S = \mathbf{Y}_{\text{trn}}(\mathcal{S}, :)$.

This DEIM-based pilot selection method offers key advantages over other selection approaches. First, by design, the pilots chosen by DEIM yield small values of the error factor η_S , and thus the bound in (14). Because of this, and the fact that we expect the data in \mathbf{Y}_{obs} to exist near the same low-dimensional subspace spanned by \mathbf{Y}_{trn} , measurements from the non-pilot datastreams can be approximated from the pilots with high fidelity. Second, spurious retraining can be avoided by periodically recomputing $\eta_S \sigma_{K+1}$ for the current set of pilots \mathcal{S} but using a new batch of online data from all datastreams. So long as the heuristic ‘‘bound’’ $\eta_S \sigma_{K+1}$ remains below an acceptable threshold, the current configuration of pilots is accepted. Otherwise, retraining is needed: DEIM is applied to \mathbf{Y}_{obs} to select a new set of pilots.

Numerical Tests. We test the adaptive DEIM-based training of pilot datastreams using 120 s of ambient voltage magnitudes $\mathbf{Y}_{\text{trn}} \in \mathbb{R}^{68 \times 12000}$ generated at 100 Hz using the NETSNYPS 68-bus, 16-machine test system. To observe the evolution of the error factor η_S and the bound $\eta_S \sigma_{K+1}$ throughout the training procedure, we run DEIM for $K = 10$ iterations. We compare the DEIM-based training with pilot configurations computed from \mathbf{Y}_{trn} using the QDEIM, MILP, and RAND selection schemes described in Section III-B. Because these

other schemes are not inherently iterative like DEIM, we run them repeatedly for each fixed size $K = 1, 2, \dots, 10$ of \mathcal{S} (and thus, unlike DEIM, the resulting index sets need not be nested).

Figure 3 shows the evolution of η_S and $\eta_S \sigma_{K+1}$ as K , the number of pilots, grows. We observe that these quantities steadily decrease with K as each new pilot is selected by DEIM and QDEIM. For the MILP- and RAND-based selections, both the error factor and thus the error bound tend to oscillate and generally *increase* as more pilots are added. Had DEIM not been forced to run for 10 iterations, it would have met the tolerance $\tau = 5 \times 10^{-2}$ after just $K = 5$ iterations.

B. Online Monitoring and Detection Using the Bound (14)

After using \mathbf{Y}_{trn} to determine the K pilot streams in \mathcal{S} and the matrix \mathbf{Z}_S offline, dimension reduction of the online data \mathbf{Y}_{obs} is achieved in real time via a rank- K ID \mathbf{Y}_S . Suppose we want to recover the data from one of the non-pilot streams $i \notin \mathcal{S}$ at the j -th time snapshot, i.e., $\mathbf{Y}_{\text{obs}}(i, j)$. To recover $\mathbf{Y}_{\text{obs}}(i, j)$, data from each of the K pilot streams $\mathbf{Y}_{\text{obs}}(s_k, j)$, $k = 1, \dots, K$, are combined according to

$$\mathbf{Y}_{\text{obs}}(i, j) \approx \mathbf{Y}_S(i, j) := \sum_{k=1}^K \mathbf{Z}_S(i, k) \mathbf{Y}_{\text{obs}}(s_k, j). \quad (17)$$

We emphasize that the datastreams indicated by \mathcal{S} are chosen based on the offline data \mathbf{Y}_{trn} , but the actual *online* datastreams in \mathbf{Y}_{obs} are used to form the reconstruction (17). Because the training and online data are not the same, $\eta_S \sigma_{K+1}$ (from \mathbf{Y}_{trn}) does not provide a theoretically rigorous upper bound for $|\mathbf{Y}_{\text{obs}}(i, j) - \mathbf{Y}_S(i, j)|$, the online reconstruction error for the j -th sample of the non-pilot stream $i \notin \mathcal{S}$. However, the factor $\eta_S \sigma_{K+1}$ can serve as an *estimator* of the online reconstruction error: since the training data \mathbf{Y}_{trn} reflect normal operating conditions, we expect the low-dimensional subspaces spanned by \mathbf{Y}_{trn} and \mathbf{Y}_{obs} to be similar.

What happens if the error estimator $\eta_S \sigma_{K+1}$ is no longer accurate during real-time operations? That is, what if, for a parameter $\theta > 0$, the actual reconstruction error satisfies

$$|\mathbf{Y}_{\text{obs}}(i, j) - \mathbf{Y}_S(i, j)| > \theta \eta_S \sigma_{K+1} \quad (18)$$

at some non-pilot $i \notin \mathcal{S}$ for the j -th sample? This violation suggests a flaw in the assumption that the low-dimensional column space of \mathbf{Y}_{obs} is close to that of \mathbf{Y}_{trn} , and thus signals

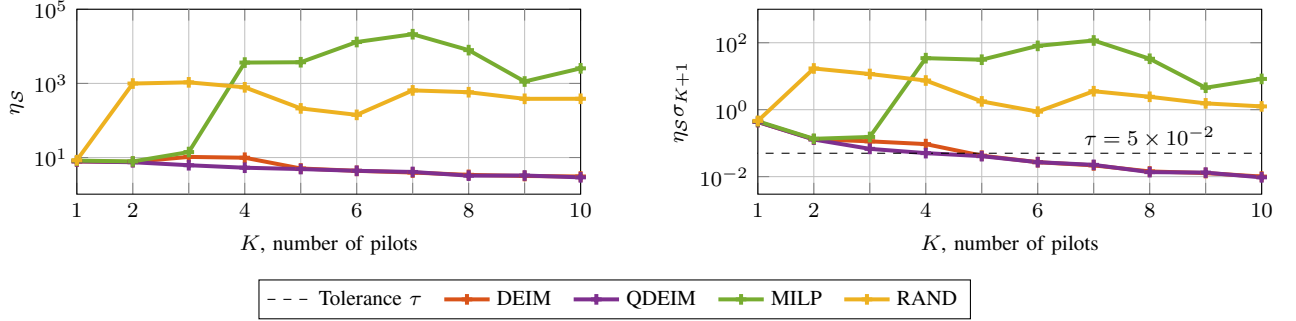


Figure 3: Evolution of the error factor η_S and the upper bound $\eta_S \sigma_{K+1}$ throughout the adaptive training as K pilots are chosen.

that there has been a fundamental change in the network's operating condition, e.g., due to a disturbance.

We propose that the deterioration of the error estimate as in (18) be used as a simple mechanism for detecting changes to the network's operating conditions. Taking the parameter $\theta > 1$ increases the chance of false negatives (FN: a change in the network occurs but goes unnoticed), whereas taking $\theta < 1$ will increase the chance of false positives (FP: a change in the network is detected where none has occurred).

Necessarily, checking (18) requires continuously monitoring the interpolatory reconstruction error at some non-pilot datastreams $i \notin \mathcal{S}$. These non-pilot datastreams can be chosen based on the geography of the network, e.g., they may be collected from PMUs that are geographically distributed, to monitor for disturbances that are localized to a subnetwork. For our tests, we let the DEIM-based training procedure continue to run for M more iterations after $\eta_S \sigma_{K+1} \leq \tau$ is satisfied, for some positive integer M . We use these M additional indices as the monitored non-pilot datastreams. Lastly, we mention that a similar detection mechanism based on the deterioration of the pilot-based reconstruction error is proposed in [5, Sec. III.B]. By comparison, our detector (18) is grounded in the theoretical upper bound on the interpolatory approximation error (14).

Numerical tests. We investigate the proposed online monitoring algorithm with two numerical tests. First, we apply the algorithm to the online simulation scenario from Section III-B, which was generated by the NETSNYPS 68-bus, 16-machine test system [29, Ch. 4]. Each bus in the network is equipped with a single PMU, each of which records the nodal voltage magnitude. The online portion of the simulation is 60 s in total; after 30 s, a three-phase fault is applied to the line connecting buses 28 and 29, and cleared 0.2 s later. To select the pilot streams, we re-run the adaptive DEIM-based training algorithm on the 120 s of training data from Section IV-A with $\tau = 0.05$. DEIM chooses $K = 5$ pilot streams, at which point the error tolerance is satisfied. For comparison, we run MILP to select $K = 5$ pilots; both configurations are reported in Table I, along with the associated error bounds $\eta_S \sigma_{K+1}$. For the same fixed K , the DEIM-based pilots produce an error bound that is *three* orders of magnitude less than the bound for the MILP-based pilots. For this experiment, we use $M = 2$ non-pilot streams: these are the next two pilots identified by DEIM after $K = 5$, and correspond to the voltage magnitudes

at buses 63 and 57.

Following training, the reconstruction errors at the non-pilot streams are monitored and compared against the error indicator $\theta \eta_S \sigma_{K+1}$ (18). For this test, we set $\theta = 1$. The non-pilot streams, along with the DEIM- and MILP-based reconstructions, before and during the disturbance, are plotted in Figure 4 along with the associated error estimators $\eta_S \sigma_{K+1}$ for each pilot configuration. Before the disturbance and during ambient operating conditions, both the DEIM- and MILP-based reconstructions are accurate and well within the error estimate. At the first sample following the line fault, the error estimator is violated according to (18) for the DEIM-based reconstruction at the non-pilot bus 63, and the fault is correctly detected. At bus 57, the estimator is very nearly violated; this motivates rescaling the estimator by values of $\theta < 1$. For the MILP-based reconstruction, the error remains within acceptable parameters according to the estimator (as η_S is excessively large), and thus no fault is detected.

For the second test, we verify the robustness of the mechanism (18) in detecting disturbances on a batch of simulation scenarios. We again test both the DEIM- and MILP-based selections. All simulations use the same 120 s of training data as in the last experiment, and so choose the same $K = 5$ pilot buses in Table I. We use the same $M = 2$ non-pilot buses 63 and 57 as in the previous experiment, which we monitor for both the DEIM and MILP tests. The experimental batch contains 84 simulations, each of which occurs over a $T_{\text{obs}} = 100$ s window. The data are voltage magnitudes recorded at each bus at a rate of 100 Hz. During each online simulation, a three-phase line fault is applied at some line in the network at a random time and cleared 0.2 s later. We classify each decision as a TP (the fault is correctly detected at one of the non-pilots within 1 s of the event according to (18)), an FP (a fault is detected outside of this window at both or one of the non-pilots, and not detected at the other), or an FN (no fault is detected at either of the non-pilots). We evaluate

Table I: $K = 5$ pilot streams as chosen by DEIM and MILP, and values of the corresponding error estimator in (14).

	s_1	s_2	s_3	s_4	s_5	$\eta_S \sigma_6$
DEIM	48	61	50	54	59	4.2391e-2
MILP	42	52	61	67	68	3.1120e+1

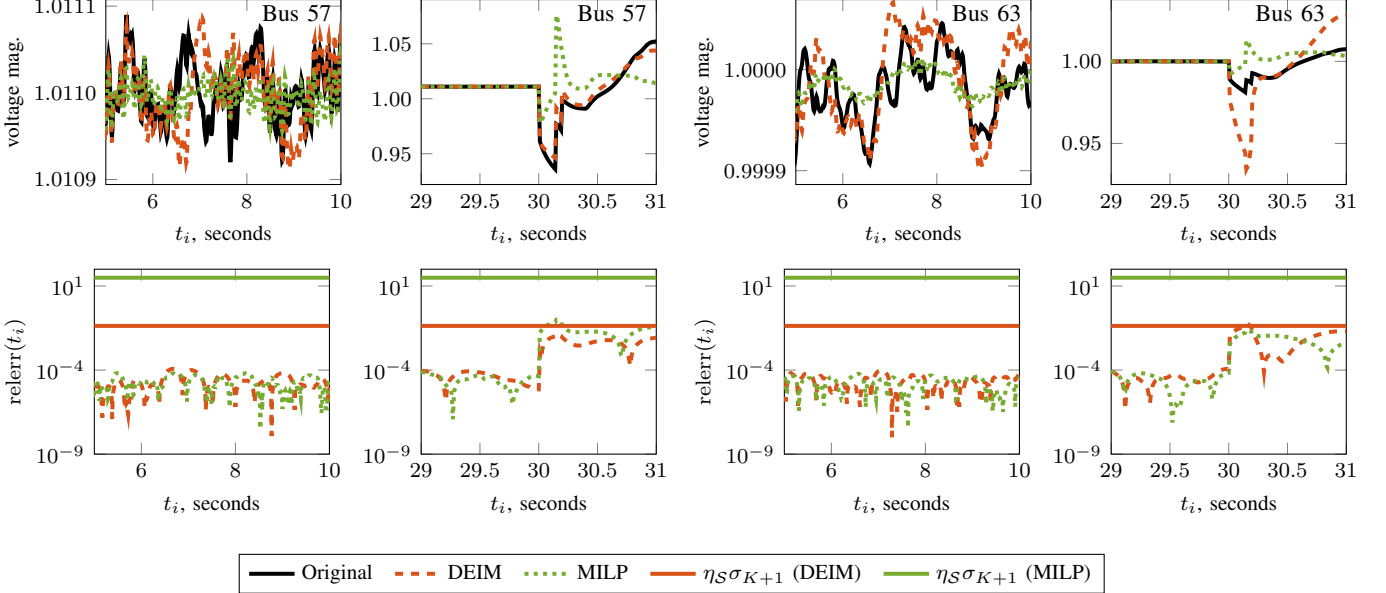


Figure 4: Interpolatory reconstruction and true data for the non-pilot datastreams at bus 57 (left) and bus 63 (right) prior to and during a three-phase fault of the line between buses 28 and 29.

the performance of the detection mechanism (18) using F_1 and F_2 scores [32], computed as

$$F_1 = \frac{2 \times \text{Precision} \times \text{Recall}}{\text{Precision} + \text{Recall}}, \quad F_2 = \frac{5 \times \text{Precision} \times \text{Recall}}{4 \times \text{Precision} + \text{Recall}},$$

for Precision = TP / (TP + FP), Recall = TP / (TP + FN). Values close to 1 indicate a reliable detection mechanism.

We compute the F_1 and F_2 scores for four different detection mechanisms: (18) using the DEIM-based pilots with $\theta = 1$ and $\theta = 10^{-2}$, and (18) using the MILP-based pilots with the same two values of θ . These scores, along with the associated Precision and Recall, are recorded in Table II. We observe a substantial improvement across all metrics when θ is decreased from 1 to 10^{-2} . For the MILP-based pilot configuration, this improvement is extremely significant. For both values of θ , the DEIM-based pilots outperform the MILP-based pilots drastically in almost all metrics, due to the comparatively lower magnitude error bound induced by DEIM.

C. Event localization using DEIM

After a disturbance occurs, it is imperative to find its source, e.g., the buses adjacent to a faulted line, quickly, so system operators can take corrective action to prevent cascading

Table II: Precision, Recall, F_1 and F_2 scores for the event detection mechanism (18) using the DEIM- and MILP-based pilots for $\theta = 1$ and 10^{-2} . The largest scores in each row are highlighted in **boldface**.

	DEIM $\theta = 1$	DEIM $\theta = 10^{-2}$	MILP $\theta = 1$	MILP $\theta = 10^{-2}$
Precision	0.8378	0.9506	0.0000	0.6000
Recall	0.8986	1.0000	0.0000	0.2112
F_1	0.8671	0.9747	0.0000	0.3125
F_2	0.8857	0.9897	0.0000	0.2427

failures. Numerous works have explored the event location problem; see, e.g. [8], [11], [12]. As an alternative to these approaches, we propose using the DEIM algorithm to localize the source of disturbances. Specifically, once a disturbance has been detected using (18) (or any other detection mechanism), DEIM can be applied to a batch of data containing the transient system response following the disturbance. In our tests, as little as 1 s of data is needed to localize the event.

Numerical tests. We demonstrate the ability of DEIM to localize disturbances using the same simulation dataset from Section IV-B. For comparison, we use the data-driven energy-based (EB) criterion for localizing affected buses from [8]. For each scenario, we assume that an event alert has been correctly issued. We then aggregate 0.5 s of data prior to the event and 1.0 s of data directly after the event into the matrix \mathbf{Y} . Before attempting to localize the source of the event, this matrix is preprocessed by removing the mean of the pre-event data as in [8]. We apply DEIM, QDEIM, and EB to the leading k left singular vectors \mathbf{U}_k of \mathbf{Y} to select up to $k = 1, 2, \dots, 8$ rows, each of which corresponds to a particular PMU in the network. If *both* buses connected to the faulted line are found within these k indices, we classify the method as having correctly localized the source of the event. This process is repeated for each of the 83 event simulation scenarios.

The percentages of these event scenarios for which DEIM, QDEIM, or EB correctly identified its source within k indices are plotted in Figure 5. For $k \geq 4$, all methods localize the source of the faulted line with greater than 80 percent accuracy, and 90 percent accuracy for $k \geq 5$. Thus, given the freedom to select enough indices, our QDEIM-based localization strategy correctly identifies both affiliate buses in all scenarios, and performs marginally better than the reference approach in [8].

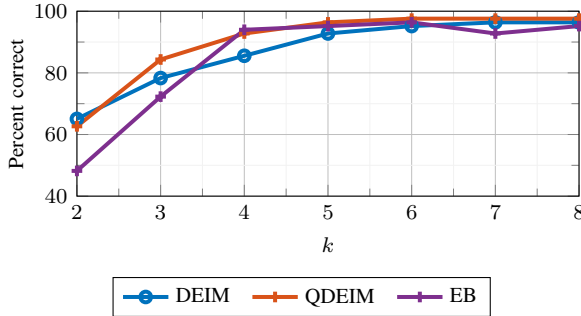


Figure 5: Percentage of event simulations (83 experiments) in which the indicated method correctly identified both buses associated with the faulted line in the first k indices for $k = 2, \dots, 8$.

V. CONCLUSIONS

Interpolatory matrix decompositions (IDs) and the discrete empirical interpolation method (DEIM) provide effective tools for PMU data compression, network monitoring, and event detection. We have shown that IDs give effective low-rank approximations of PMU data, particularly for time-sensitive and bandwidth-limited applications such as wide-area monitoring. IDs can be maintained in real-time while interacting with $K \ll N$ pilot streams or $K \ll T$ pilot snapshots. Casting data compression in the mathematical framework of IDs provides a rigorous upper bound (14) on the training error. To identify pilot buses for online monitoring, we have employed DEIM, a greedy method designed to give favorable error bounds. DEIM can be applied during offline training to adaptively select pilots until the bound (14) falls below a user's tolerance, giving an estimate for the online reconstruction error. Any significant deterioration in this error estimate, as in (18), signals a notable change to the network's operating status compared to training conditions, providing a mechanism to detect disturbances. We have illustrated that DEIM and its QDEIM variant can be used to localize the source of disturbances quite robustly.

REFERENCES

- R. Klump, P. Agarwal, J. E. Tate, and H. Khurana, "Lossless compression of synchronized phasor measurements," in *IEEE Power and Energy Society General Meeting*. IEEE, 2010, pp. 1–7.
- P. H. Gadde, M. Biswal, S. Brahma, and H. Cao, "Efficient compression of PMU data in WAMS," *IEEE Trans. Smart Grid*, vol. 7, no. 5, pp. 2406–2413, 2016.
- S. Das and T. S. Sidhu, "Application of compressive sampling in synchrophasor data communication in WAMS," *IEEE Trans. Ind. Informat.*, vol. 10, no. 1, pp. 450–460, 2013.
- S. Das, "Sub-Nyquist rate ADC sampling in digital relays and PMUs: Advantages and challenges," in *2016 IEEE 6th International Conference on Power Systems (ICPS)*. IEEE, 2016, pp. 1–6.
- L. Xie, Y. Chen, and P. Kumar, "Dimensionality reduction of synchrophasor data for early event detection: Linearized analysis," *IEEE Trans. Power Syst.*, vol. 29, no. 6, pp. 2784–2794, 2014.
- N. Dahal, R. L. King, and V. Madani, "Online dimension reduction of synchrophasor data," in *PES T&D 2012*, 2012, pp. 1–7.
- M. Wang, J. H. Chow, D. Osipov, S. Konstantinopoulos, S. Zhang, E. Farantatos, and M. Patel, "Review of low-rank data-driven methods applied to synchrophasor measurement," *IEEE Open Access J. Power Energy*, vol. 8, pp. 532–542, 2021.
- W. Li, M. Wang, and J. H. Chow, "Real-time event identification through low-dimensional subspace characterization of high-dimensional synchrophasor data," *IEEE Trans. Power Syst.*, vol. 33, no. 5, pp. 4937–4947, 2018.
- G. H. Golub and C. F. Van Loan, *Matrix Computations*, 4th ed. Baltimore: Johns Hopkins University Press, 2012.
- I. T. Jolliffe, *Principal Component Analysis*, 2nd ed. New York: Springer, 2002.
- Z. Wang, Y. Zhang, and J. Zhang, "Principal components fault location based on WAMS/PMU measure system," in *2011 IEEE Power and Energy Society General Meeting*. IEEE, 2011, pp. 1–5.
- X. Liu, D. Laverty, R. Best, K. Li, D. Morrow, and S. McLoone, "Principal component analysis of wide-area phasor measurements for islanding detection—a geometric view," *IEEE Trans. Power Del.*, vol. 30, no. 2, pp. 976–985, 2015.
- M. Rafferty, X. Liu, D. M. Laverty, and S. McLoone, "Real-time multiple event detection and classification using moving window PCA," *IEEE Trans. Smart Grid*, vol. 7, no. 5, pp. 2537–2548, 2016.
- P. Gao, M. Wang, S. G. Ghiocel, J. H. Chow, B. Fardanesh, and G. Stefanopoulos, "Missing data recovery by exploiting low-dimensionality in power system synchrophasor measurements," *IEEE Trans. Power Syst.*, vol. 31, no. 2, pp. 1006–1013, 2015.
- Y. Hao, M. Wang, J. H. Chow, E. Farantatos, and M. Patel, "Modelless data quality improvement of streaming synchrophasor measurements by exploiting the low-rank Hankel structure," *IEEE Trans. Power Syst.*, vol. 33, no. 6, pp. 6966–6977, 2018.
- X. Kong, B. Foggo, K. Yamashita, and N. Yu, "Online voltage event detection using synchrophasor data with structured sparsity-inducing norms," *IEEE Trans. Power Syst.*, vol. 37, no. 5, pp. 3506–3515, 2021.
- M. W. Mahoney and P. Drineas, "CUR matrix decompositions for improved data analysis," *Proc. Nat. Acad. Sci.*, vol. 106, pp. 697–702, 2009.
- D. C. Sorensen and M. Embree, "A DEIM induced CUR factorization," *SIAM J. Sci. Comput.*, vol. 38, pp. A1454–A1482, 2016.
- E. Liberty, F. Woolfe, P.-G. Martinsson, V. Rokhlin, and M. Tygert, "Randomized algorithms for the low-rank approximation of matrices," *Proc. Nat. Acad. Sci.*, vol. 104, pp. 20 167–20 172, 2007.
- Y. Dong and P.-G. Martinsson, "Simpler is better: a comparative study of randomized pivoting algorithms for CUR and interpolative decompositions," *Adv. Comput. Math.*, vol. 49, 2023.
- G. W. Stewart, "Four algorithms for the efficient computation of truncated pivoted QR approximations to a sparse matrix," *Numer. Math.*, vol. 83, pp. 313–323, 1999.
- S. Liu, Y. Zhao, Z. Lin, Y. Liu, Y. Ding, L. Yang, and S. Yi, "Data-driven event detection of power systems based on unequal-interval reduction of PMU data and local outlier factor," *IEEE Trans. Smart Grid*, vol. 11, no. 2, pp. 1630–1643, 2019.
- S. Chaturantabut and D. C. Sorensen, "Nonlinear model reduction via discrete empirical interpolation," *SIAM J. Sci. Comput.*, vol. 32, pp. 2737–2764, 2010.
- M. Barrault, Y. Maday, N. C. Nguyen, and A. T. Patera, "An empirical interpolation method: application to efficient reduced-basis discretization of partial differential equations," *C. R. Math. Acad. Sci. Paris*, vol. 339, no. 9, pp. 667–672, 2004.
- Z. Drmac and S. Gugercin, "A new selection operator for the discrete empirical interpolation method—improved a priori error bound and extensions," *SIAM J. Sci. Comput.*, vol. 38, pp. A631–A648, 2016.
- E. P. Hendryx Lyons, "The discrete empirical interpolation method in class identification and data summarization," *WIREs Comput. Stat.*, vol. 16, no. 3, p. e1653, 2024.
- Y. P. Hong and C.-T. Pan, "Rank-revealing QR factorizations and the singular value decomposition," *Math. Comp.*, vol. 58, pp. 213–232, 1992.
- S. Reiter, "Code, data and results for numerical experiments in: 'Interpolatory Approximations of PMU Data: Dimension Reduction and Pilot Selection' (version 1.0)," Oct. 2025.
- B. Pal and B. Chaudhuri, *Robust Control in Power Systems*. New York: Springer, 2005.
- J. H. Chow and K. W. Cheung, "A toolbox for power system dynamics and control engineering education and research," *IEEE Trans. Power Syst.*, vol. 7, no. 4, pp. 1559–1564, 1992.
- M. Wang, J. H. Chow, Y. Hao, S. Zhang, W. Li, R. Wang, P. Gao, C. Lackner, E. Farantatos, and M. Patel, "A low-rank framework of PMU data recovery and event identification," in *2019 International Conference on Smart Grid Synchronized Measurements and Analytics (SGSMA)*, 2019, pp. 1–9.
- C. Goutte and E. Gaussier, "A probabilistic interpretation of precision, recall and F-score, with implication for evaluation," in *European Conference on Information Retrieval*. Springer, 2005, pp. 345–359.